TECHNICAL MEMORANDUMS

NATIONAL ADVISORY COMMITTEE FOR AERONAUTICS

No. 638

# THE DANGEROUS SIDESLIP OF A STALLED AIRPLANE
# AND ITS PREVENTION

By Richard Fuchs and Wilhelm Schmidt

Zeitschrift für Flugtechnik und Motorluftschiffahrt
Vol. 22, No. 13, July 14, 1931
Verlag von R. Oldenbourg, München und Berlin



Washington
September, 1931

NATIONAL ADVISORY COMMITTEE FOR AERONAUTICS

TECHNICAL MEMORANDUM NO. 638

# THE DANGEROUS SIDESLIP OF A STALLED AIRPLANE AND ITS PREVENTION*

By Richard Fuchs and Wilhelm Schmidt

A large proportion of all airplane accidents occur shortly after taking off or shortly before landing. They may be of two kinds: It may happen that the airplane shows a tendency to slip over the wing without the pilot having a chance to take protective measures against it by control action. Then again, there are cases of sudden nosing over without the pilot being in a position to counteract it. This investigation covers only that phase of the problem which deals with the sideslip. We examine into the circumstances under which this occurs, study the behavior of present-day airplane types (monoplane, conventional and staggered biplane) therein and endeavor to find a solution whereby this danger may be avoided.

Occasionally the opinion is voiced that this sideslip could be prevented by using a wing whose lift maximum is at the highest possible angle of attack and by making provision, through a limitation in elevator displacement, so that an equilibrium of the moments about the lateral axis becomes impossible at the high angles of attack pertaining to those beyond the lift maximum.

But these measures are no absolute preventative, as we shall prove.

A sudden increase in angle of attack which may be altogether independent from an actuation of the elevator may be due to a straight upward directed wind squall. Thus, referring to Figure 1, a vertical squall of only 5 m/s (16.4 ft./sec.), with a landing speed of 30 m/s (98.4 ft./sec.) already produces a 9.5° increase in angle of attack. Even a vertical squall of merely 3 m/s (9.8 ft./sec.) would raise this angle to a figure which would be beyond that of the maximum lift.

---

*"Das gefährliche seitliche Kippen eines Flugzeuges über den Flügel und seine Beeinflussung." From Zeitschrift für Flugtechnik und Motorluftschiffahrt, July 14, 1931, pp. 393-400.

Again, an abrupt decrease in the relative wind velocity of an airplane can readily raise the angle of attack. For example: Let the examined low wing Junkers A 35 (references 1 and 2) monoplane land at an angle of attack $\alpha = 13^\circ$ in a straight glide, or, in other words, at an angle still $4^\circ$ below that of the maximum lift of the whole airplane. Assume a landing speed 26 m/s (85.3 ft./sec.), which in still air is equivalent to the velocity at which the air strikes the airplane. An assumedly sudden horizontal squall of 7 m/s (23 ft./sec.) strikes the airplane from the rear, thus lowering the relative wind velocity of the airplane to 19 m/s (62.3 ft./sec.). We shall designate this by $v^*$. A similar increase in angle of attack could occur when the airplane lands in the wind and the latter suddenly becalms. In order to follow the changed attitude of the airplane due to a change in relative wind velocity the terms in the differential equations of motion embodying the aerodynamic forces and moments must be changed to read $v^*$ instead of $v$. The result of the numerical integration is graphed in Figure 2. The angle of attack $\alpha = 15^\circ$ pertaining to approximately the maximum wing lift is already exceeded after 0.2 s without the pilot's volition, even if the elevator displacement is restricted.

This passage near the ground of the angle of attack beyond that of the maximum lift constitutes the danger of the undamped sideslip. In Figure 3 the moments about the longitudinal axis have been plotted against a rotation about the path axis for various angles of attack. The ensuing moments below the stalling angle are, as seen, positive; that is, active against the indicated rotation, while those beyond the stall at first become negative, that is, accelerate an incipient rotation.

Now, however, we assume that the angle of attack has exceeded the value for maximum wing lift only, and subsequently examine the reaction of the low wing Junkers monoplane landing in a straight glide against any arbitrary disturbance.

Foremost among the disturbances are the rotational speeds $\dot{\mu}$, $\dot{\tau}$, and $\dot{\alpha}$, introduced as temporary initial rotations $\dot{\mu}_0$, $\dot{\tau}_0$, and $\dot{\alpha}_0$, and which may be visualized as having been set up by corresponding temporary control displacements or wind squalls temporarily acting at the end of the fuselage and the wing tip.

The result of the very accurately executed numerical integration of the fundamental equations is appended in Figures 4 to 6. The result of introducing an initial rotation $\dot{\mu}_0$ is not only an expected angle of bank $\mu$ in Figure 4, but an angle of yaw $\tau$ as well, and the angle of attack remains, for the present at least, practically constant.

The initiated disturbance $\tau_0$, in Figure 5, yields a similar result. The angle of attack changes at first very little. Whereas an arbitrary initial disturbance, composed of say, $\dot{\mu}_0$ and $\dot{\alpha}_0$, effects a change in angle of attack, the peculiar temporal character of the angles of bank and yaw is maintained, according to Figure 6.

The behavior of $\alpha$ which is examined here, is bound up with the airplane motion by great static longitudinal stability. As a matter of fact, we have here an airplane attitude with appreciably high static longitudinal stability. In this attitude the motion is split up in a slow C.G. motion by constant $\alpha$ (Lanchester's phugoid theory)* (reference 3) and a rapid torsional vibration about the lateral axis by unchanging flight path. It is apparent that the torsional vibrations set up by asymmetrical disturbances do not effect any essential change. As far as the change in angle of bank and yaw is concerned, it is practically immaterial whether $\alpha$ changes also or not, and it is seen that the asymmetric rotary motion is also nearly independent of the symmetrical motion.

Accordingly, the sideslip following an arbitrary disturbance may be conceived as a combined rolling and yawing motion, which is practically independent of the pitching motion, thus enabling us to separate the pitching motion from the rolling and yawing motion, to which the following is confined exclusively.

Referring to Figure 4, the total motion during sideslip consists primarily of a rotation $\Omega_x$ about the path axis and a rotation $\Omega_{\underline{y}_1}$ around the path vertical axis placed in the symmetrical plane of the aircraft. The forces and the moment about the lateral axis change but little at the beginning of sideslip because the angle of attack remains practically constant and the sideslip as well as the total rotation is relatively small in contrast to the moments about the longitudinal and the normal axis which undergo marked changes even if sideslip and rotation

*The possibility of separation was first indicated by Reissner.

are small. For the subsequent investigation it is advisable to introduce the practically constant angle $\alpha$ as parameter, and to consider the two variable nondimensional factors $\underline{K}$ and $\underline{L}$ of the moments about the longitudinal and normal axis, respectively, as being solely dependent on $\tau$, $\frac{b\Omega_x}{2\ v}$ and $\frac{b\Omega_{\underline{y}_1}}{2\ v}$. Strictly speaking, the two moments should be considered as being simultaneously dependent on these values, but for lack of wind-tunnel data of such kind, we assume both moments as being linearly dependent on these figures which, in this case is of no moment because the calculation is confined to short time intervals. Figures 7 and 8 afford an illustration of the $\underline{K}_{F_\tau}$ and $\underline{L}_{F_\tau}$ moments of the wing only due to sideslip plotted against the angle of yaw; the angle of attack is shown as parameter. They are taken from a British report (reference 4) because there are no German experiments available up to such high angles of attack and yaw.

The $\underline{K}_{F\Omega_x}$ and the $\underline{L}_{F\Omega_x}$ moments due to a rotation about the path axis are defined in the usual manner by calculation as, for instance, for the single wing of the Junkers monoplane, and appended in Figures 3 and 9 with respect to $\frac{b\Omega_x}{2\ v}$ and with $\alpha$ as parameter. Their dependence on the shape of the wing is very pronounced. (Reference 5.) A calculation of an individual wing of almost constant chord and section yields for the $\underline{K}_{F\Omega_{\underline{y}_1}}$ and $\underline{L}_{F\Omega_{\underline{y}_1}}$ moments, due to a rotation $\Omega_{\underline{y}_1}$ about the lift axis the following:

$$\underline{K}_{F\Omega_{\underline{y}_1}} = \frac{b^2}{3F}\, c_{n_F}\, \frac{b\Omega_{\underline{y}_1}}{2v} \qquad \underline{L}_{F\Omega_{\underline{y}_1}} = \frac{b^2}{3F}\, c_{t_F}\, \frac{b\Omega_{\underline{y}_1}}{2v}.$$

Figures 10 and 11 shows this effect for the low wing monoplane.

The $\underline{L}^*$ coefficient due to the moment of fuselage and vertical tail surfaces about the normal axis may be written as

$$\underline{L}^* = \frac{F^*\ l^*}{F\ t_1}\, c_n{}^*\ (\alpha^*),$$

where $c_n^* (\alpha^*)$ signifies that $c_n^*$ is dependent on the angle $\alpha^*$ at which the air strikes the end of the fuselage and the vertical tail surfaces. The validity is practically

$$\alpha^* = \tau + \frac{l^* \, \Omega_{\underline{y}_1}}{v}$$

The $c_n^*$ coefficient of the normal force applying at the end of the fuselage and the vertical tail group is, for lack of experimental data, replaced by the corresponding coefficient of a flat, square plate.

The curves of the moments about the longitudinal and the normal axis, treated above, with respect to $\tau$, $\frac{b\Omega_{\underline{x}}}{2\,v}$ and $\frac{b\Omega_{\underline{y}_1}}{2\,v}$ can be equated for the pertinent range by a straight line as follows:

$$\underline{K}_{F_\tau} = m_1 \, \tau \qquad \underline{L}_{F_\tau} = m_2 \, \tau$$

$$\underline{K}_{F_{\Omega_x}} = m_3 \, \frac{b\Omega_{\underline{x}}}{2\,v} \qquad \underline{L}_{F_{\Omega_x}} = m_4 \, \frac{b\Omega_{\underline{x}}}{2\,v}$$

$$\underline{K}_{F_{\Omega_{\underline{y}_1}}} = m_5 \, \frac{b\Omega_{\underline{y}_1}}{2v} \qquad \underline{L}_{F_{\Omega_{\underline{y}_1}}} = m_6 \, \frac{b\Omega_{\underline{y}_1}}{2v}$$

The moment about the normal axis due to the fuselage and the vertical tail surfaces may be expressed as

$$\underline{L}^* = m_7 \left( \frac{F^* \, l^*}{F \, t_1} \, \tau + \frac{2F^* \, l^{*2}}{b \, F \, t_1} \, \frac{b\Omega_{\underline{y}_1}}{2\,v} \right)$$

so as to yield

$$\underline{K} = m_1 \, \tau + m_3 \, \frac{b\Omega_{\underline{x}}}{2v} + m_5 \, \frac{b\Omega_{\underline{y}}}{2v} \tag{1}$$

$$\underline{L} = \left( m_2 + \frac{F^* \, l^*}{F \, t_1} \, m_7 \right) \tau + m_4 \, \frac{b\Omega_{\underline{x}}}{2\,v} + \left( m_6 + \frac{2F^* \, l^{*2}}{b \, F \, t_1} \, m_7 \right) \frac{b\Omega_{\underline{y}_1}}{2v} \tag{2}$$

Now we write equations (1) and (2) into the basic equations, replace the products of several variables by the first terms of a Taylor series and, lastly, disregard the terms which are small compared to the others, so that

$$\omega = - \frac{\gamma\ F\ v\ c_a}{2G\ \cos\varphi}\ \mu \tag{3}$$

$$\dot{\mu} = \frac{1}{\cos\alpha}\ \Omega_{\underline{x}} \tag{4}$$

$$\dot{\tau} = \frac{g\ \cos\varphi}{v\ \cos\alpha}\ \mu + \tan\alpha\ \Omega_{\underline{x}} + \Omega_{\underline{y}} \tag{5}$$

$$\dot{\Omega}_{\underline{x}} = - \frac{\gamma\ F\ t_1\ v^2}{2\ g\ J_{\underline{x}}} \left(m_1\ \tau + m_3\ \frac{b\Omega_{\underline{x}}}{2\ v} + m_5\ \frac{b\Omega_{x_1}}{2v}\right) \tag{6}$$

$$\dot{\Omega}_y = - \frac{\gamma\ F\ t_1\ v^2}{2\ g\ J_y} \left[\left(m_2 + \frac{F^*\ l^*}{F\ t_1}\ m_7\right)\tau + m_4\ \frac{b\Omega_{\underline{y}_1}}{2v} + \right.$$

$$\left. + \left(m_6 + \frac{2\ F^*\ l^{*2}}{b\ F\ t_1}\ m_7\right) \frac{b\Omega_{\underline{y}_1}}{2\ v}\right] \tag{7}$$

whereby

$$\Omega_x = \dot{\mu} - \dot{\tau}\ \sin\alpha \tag{8}$$

$$\Omega_{\underline{y}_1} = \omega\ \cos\varphi + \dot{\tau}\ \cos\alpha \tag{9}$$

Equations (3) to (9) may be combined as

$$\dot{\Omega}_{\underline{x}} = a_1\ \tau + b_1\ \dot{\tau} + c_1\ \mu + d_1\ \dot{\mu} \tag{10}$$

$$\dot{\Omega}_{\underline{y}} = a_2\ \tau + b_2\ \dot{\tau} + c_2\ \mu + d_2\ \dot{\mu} \tag{11}$$

$$\dot{\tau} = c_3\ \mu + e_3\ \Omega_{\underline{x}} + \Omega_{\underline{y}} \tag{12}$$

$$\dot{\mu} = e_4\ \Omega_{\underline{x}} \tag{13}$$

Herein:

$$a_1 = -\frac{\gamma\ F\ t_1\ v^2}{2\ g\ J_x}\ m_1$$

$$b_1 = \frac{\gamma\ b\ F\ t_1\ v\ \cos\alpha}{4\ g\ J_x}\ (\tan\alpha\ m_3 - m_5)$$

$$c_1 = \frac{\gamma^2\ b\ F^2\ t_1\ v^2\ c_a}{8\ g\ G\ J_x}\ m_5$$

$$d_1 = -\frac{\gamma\ b\ F\ t_1\ v}{4\ g\ J_x}\ m_3$$

$$a_2 = -\frac{\gamma\ F\ t_1\ v^2}{2\ g\ J_y}\left(m_2 + \frac{F^*\ l^*}{F\ t_1}\ m_7\right)$$

$$b_2 = \frac{\gamma\ b\ F\ t_1\ v\ \cos\alpha}{4\ g\ J_y}\left(\tan\alpha\ m_4 - m_6 - \frac{2\ F^*\ l^{*2}}{b\ F\ t_1}\ m_7\right)$$

$$c_2 = \frac{\gamma^2\ b\ F^2\ t_1\ v^2\ c_a}{8\ g\ G\ J_y}\left(m_6 + \frac{2\ F^*\ l^{*2}}{b\ F\ t_1}\ m_7\right)$$

$$d_2 = -\frac{\gamma\ b\ F\ t_1\ v}{4\ g\ J_y}\ m_4$$

$$c_3 = \frac{g\ \cos\varphi}{v\ \cos\alpha}$$

$$e_3 = \tan\alpha$$

$$e_4 = \frac{1}{\cos\alpha}$$

Equations (10) to (13) may be formulated as

$$\ddot{\mu} + p_1\ \dot{\mu} + q_1\ \mu + \quad r_1\ \dot{\tau} + s_1\ \tau = 0 \qquad (14)$$

$$p_2\ \dot{\mu} + q_2\ \mu + \ddot{\tau} + r_2\ \dot{\tau} + s_2\ \tau = 0 \qquad (15)$$

whereby

$$p_1 = -\ d_1\ e_4$$

$$q_1 = -\ c_1\ e_4$$

$$r_1 = - b_1 e_4$$

$$s_1 = - a_1 e_4$$

$$p_2 = - (c_3 + d_1 e_3 + d_2)$$

$$q_2 = - (c_1 e_3 + c_2)$$

$$r_2 = - (b_1 e_3 + b_2)$$

$$s_2 = - (a_1 e_3 + a_2)$$

Inserting $\mu$ and $\tau \approx e^{\lambda t}$ into (14) and (15) the interpretation of $\lambda$ is obtained by means of

$$\begin{vmatrix} \lambda^2 + p_1 \lambda + q_1 & r_1 \lambda + s_1 \\ p_2 \lambda + q_2 & \lambda^2 + r_2 \lambda + s_2 \end{vmatrix} = 0,$$

or

$$\lambda^4 + A_1 \lambda^3 + A_2 \lambda^2 + A_3 \lambda + A_4 = 0 \tag{16}$$

with

$$A_1 = p_1 + r_2$$

$$= \frac{\gamma b F t_1 v \cos\alpha}{4 g J_{\underline{x}}} \left[ m_3 + \tan\alpha\, m_5 - \frac{J_{\underline{x}}}{J_{\underline{y}}} \left( \tan\alpha\, m_4 - m_6 - \frac{2 F^* l^{*2}}{b F t_1} m_7 \right) \right] \tag{17}$$

$$A_2 = p_1 r_2 - p_2 r_1 + q_1 + s_2$$

$$= \left( \frac{\gamma b F t_1 v}{4 g} \right)^2 \frac{1}{J_{\underline{x}} J_{\underline{y}}} \left[ \frac{8 g J_{\underline{y}} \tan\alpha}{\gamma b^2 F t_1} m_1 + \left( m_6 + \frac{2 F^* l^{*2}}{b F t_1} m_7 \right) m_3 - m_4 m_5 + \frac{8 g J_{\underline{x}}}{\gamma b^2 F t_1} \left( m_2 + \frac{F^* l^*}{F t_1} m_7 \right) \right] \tag{18}$$

$$A_3 = p_1 \; s_2 - p_2 \; s_1 + q_1 \; r_2 - q_2 \; r_1$$

$$= \left(\frac{\gamma F t_1 v}{2\,g}\right)^2 \frac{b\ v}{2\ J_{\underline{x}}\ J_{\underline{y}}\ \cos\alpha} \left[\left(\frac{4g^2 J_{\underline{y}}\ \cos\varphi}{\gamma b F t_1 v^2 \cos\alpha} - m_4\right) m_1 \right.$$

$$\left. + \left(m^2 + \frac{F^*\ l^*}{F\ t_1}\, m_7\right) m_3 + \frac{\gamma b F c_a\ \sin\alpha}{4\ G}\, m_4\ m_5\right] \quad (19)$$

$$A_4 = q_1 \; s_2 - q_2 \; s_1$$

$$= \left(\frac{\gamma F t_1 v^2}{4\ g}\right)^2 \frac{\gamma b F\ c_a}{J_{\underline{x}}\ J_{\underline{y}}\ G\ \cos\alpha} \left[\left(m_6 + \frac{2\ F^*\ l^{*2}}{b\ F\ t_1}\, m_7\right) m_1 \right.$$

$$\left. - \left(m^2 + \frac{2\ F^*\ l^*}{F\ t_1}\, m_7\right) m_5\right] \quad (20)$$

In order to check the agreement of this solution with the numerical integration without any omissions, the examined low-wing monoplane was used as actual example for a mathematical determination of $\mu$ and $\tau$.

The following data are used as basis:

$$\alpha = 20^\circ \quad c_a = 1.29 \quad c_w = 0.31 \quad \varphi = -13.5^\circ$$

$$\gamma = 1.20\ \mathrm{kg/m^3} \quad v = 25.8\ \mathrm{m/s} \quad \mu_o = 0^\circ \quad \tau_o = 0^\circ \quad \dot{\tau}_o = 0.$$

$\dot{\mu}_o \neq 0$, a passing asymmetric squall, has assumedly imparted to the airplane an initial rotation about the path axis.

$$m_1 = +1.2 \quad m_3 = -2.7 \quad m_5 = +3.5 \quad m_7 = +4.0$$

$$m_2 = +0.1 \quad m_4 = +0.8 \quad m_6 = -0.5.$$

It yields:

$$\frac{\mu}{\dot{\mu}_o} = 0.239\ e^{5.77t} - 0.185\ e^{-0.39t} -$$

$$- e^{-0.59t}\ (0.054\ \cos 2.38t + 0.218\ \sin 2.38t) \quad (21)$$

$$\frac{\tau}{\dot{\mu}_o} = 0.047\ e^{5.77t} - 0.016\ e^{-0.39t} -$$

$$- e^{-0.59t}\ (0.030\ \cos 2.38t + 0.166\ \sin 2.38t) \quad (22)$$

Figure 12 shows $\frac{\mu}{\dot{\mu}_0}$ (bank) and $\frac{\tau}{\dot{\mu}_0}$ (yaw) plotted against the time. Both curves are in satisfactory agreement throughout with those of the integration and disclose the characteristic behavior.

The substitution of a development according to the powers of $t$ for the solutions of (14) and (15) reveals the decisive significance of the coefficients $p_1$, $r_1$, $p_2$ and $r_2$ at the very beginning. But because of the magnitude of $p_1$ and $r_1$ against $p_2$ and $r_2$, $\mu$ and $\dot{\mu}$ must always be large with respect to $\tau$ and $\tau$ even for arbitrary disturbances, in accordance with all exact calculations. Thus the omission of $\tau$ and $\dot{\tau}$ in first approximation in (14) results in a Faust formula for the behavior of $\mu$. It is

$$\frac{\mu}{\dot{\mu}_0} = \frac{1}{\lambda_1} \left(e^{\lambda_1 t} - 1\right) \tag{23}$$

where

$$\lambda_1 = \frac{\gamma\ b\ F\ t_1\ v\ m_3}{4\ g\ \cos\alpha\ J_x}$$

The value computed according to the Faust formula for the above example is also shown in Figure 12, where the typical behavior of the angle of bank is very much in evidence.

This brings us to the question as to what constructive measures may have some effect on sideslipping, i.e., increase in angle of bank $\mu$. The quantities $b$, $F$ and $t_1$ are dominant factors. Area $F$ is specified by the design; $b$ and $t$ do not occur save in the connection $b\ t_1$, i.e. essentially as the stated area $F$. $F^*$ and $l^*$ occur only in the form of $F^*\ l^*\ m_7$. So any change of these quantities is wholly equivalent to a change in $m_7$ and we can confine ourselves to a study of the changes in $J_x$ and $J_y$ and from $m_1$ to $m_7$.

In accordance with the above example, one large positive, one small negative, and two complex roots occur under the roots of the biquadratic equation (16), whose real part is negative and small. In all practical changes of normal wing design this phenomenon is typical. A change in $\mu$ and $\tau$ is essentially governed by the large positive root $\lambda_1$, and it is all a matter of finding in what manner this $\lambda_1$ can be influenced.

Reverting to the original figures of the example for $J_{\underline{x}_0}$ and $J_{\underline{y}_0}$, as well as $m_{1_0}$ to $m_{7_0}$, we post $J_{\underline{x}} = \epsilon J_{\underline{x}_0}$, $m_1 = \epsilon m_{1_0}$ etc. Then we plot the dependence of root $\lambda_1$ against $\epsilon$ for $J_{\underline{x}} = \epsilon J_{\underline{x}_0}$, for $m_1 = \epsilon m_{1_0}$ etc., for example.

Referring to Figure 13, we find that only an enlargement can lower the positive root $\lambda_1$ with respect to inertia moments $J_{\underline{x}}$ and $J_{\underline{y}}$. But it is seen that even a doubling of $J_{\underline{x}}$, which already is wholly beyond the scope of practical possibility, can lower the root no more than to about 2/3, or in other words, can have no decisive effect on the essential course of angle of bank $\mu$. A change in $m_7$, that is, in the profile pertaining to the vertical tail surfaces or in its area has no appreciable effect on $\lambda_1$. The values $m_1$, $m_2$, as well as $m_5$ and $m_6$ characterize the moments about the longitudinal and the normal axis set up by the wings as a result of sideslip and rotation about the lift axis, respectively. Although dependent on the wing shape they have, in themselves, no appreciable effect on $\lambda_1$. But a change in $m_3$ and $m_4$ influences root $\lambda_1$ very materially. Both values denote the moments about the longitudinal and normal axis, respectively, following a rotation about the path axis. They are, according to Figures 3 and 9, generally negative and positive, respectively, as soon as the stalling angle is reached. They accelerate an initiated rotation about the path axis, i.e., make autorotation possible. The smaller $m_3$ and $m_4$ are, the smaller root $\lambda_1$ becomes, that is, the smaller the accelerating moments about the longitudinal and normal axis set up by an initiated rotation about the path axis. The dominant effect of $J_{\underline{x}}$ and $m_3$ is also recognized in the Faust formula (23).

A material change in inertia moments, $J_{\underline{x}}$ and $J_{\underline{y}}$ is seldom encountered in conventional types because their enlargement would offer serious constructive difficulties. The values $m_1$ to $m_6$ are closely bound up with one another. They all change, as a rule, as soon as one is changed.

To bring out the pronounced effect of $m_3$, we use two examples: In the first it was assumedly possible to lower

$m_3$ to half in a wing structure, so that,

$$m_1 = +0.60 \qquad m_4 = +0.40 \qquad m_6 = -0.25$$

$$m_2 = +0.05 \qquad m_5 = +1.75 \qquad m_7 = +4.00.$$

We also raised $J_x$ from 300 to 375 and $J_y$ from 550 to 625 in this example.

Now we have:

$$\frac{\mu}{\dot{\mu}_o} = 0.444\ e^{2.41t} - 0.304\ e^{-0.38t} -$$

$$- e^{-0.30t}\ (0.140 \cos 4.04\ t + 0.114 \sin 4.04\ t).$$

In the second example we visualize a wing structure in which $m_7$ has already assumed a small positive value, that is, a wing free from autorotation and in accordance with it:

$$m_1 = +0.4 \qquad m_4 = 0 \qquad m_6 = 0$$

$$m_2 = 0 \qquad m_5 = +1.2 \qquad m_7 = +4.0.$$

$J_x$ and $J_y$ remain unchanged. Now,

$$\frac{\mu}{\dot{\mu}_o} = 0.461\ e^{0.37t} - 0.371\ e^{-2.21t} -$$

$$- e^{-0.58t}\ (0.090 \cos 1.80\ t + 0.024 \sin 1.80\ t).$$

Figure 14 shows the results of both examples for $\mu$ along with the normal behavior. It is readily seen that the danger of sideslipping can be effectively prevented only by the use of a wing which is proof against autorotation. (Reference 6.)

Another question thrusts itself upon one's mind - whether or not the sideslip might not be effectively influenced by appropriate control action, and for that reason we also examined the effect of the control actions on sideslipping. We assumed that the pilot notices the sideslip after one second and then attempts to counteract it by control displacements.

Aileron displacement is practically useless in all circumstances. The angle of bank continues to increase in spite of it, as Figure 15 shows. The rudder displacement is somewhat more effective. It seems to lead, according to Figure 16, to a slight damping of the sideslip. Both results agree with the British tests. (References 7 and 8.) The elevator (displacement downward) is most effective. Figure 17 shows that the angle of bank ceases to increase after a time and that the sideslip is damped. But even in this case the time - only a few seconds - does not suffice to impart a profitable magnitude to the angle of bank, before reaching the ground.

Thus the successful prevention of the dangerous sideslip resides in the above stated measures. Since any material change in inertia moment is out of the question, it becomes primarily a problem of preventing the wing from autorotating (reference 6) in the wind tunnel.

Once autorotation has been eliminated, the inertia moments lose their dangerous aspect.

According to the preceding explanations the whole motion of the airplane at the beginning of sideslip is essentially a rotation about the path axis, during which the angle of attack, as well as the rate of speed, may be assumed unchanged. Furthermore, it was seen that the angle of yaw remained absolutely small. Consequently, the danger of sideslipping can be interpreted only from the autorotation as it may be observed by a wind-tunnel test.

In order to make it possible to compare various typical airplanes with respect to sideslip, the autorotation process is followed mathematically.

The equilibrium of the moments about the path axis is expressed as

$$J_x \dot{\Omega}_x = - \frac{\gamma}{2g} v^2 F t_1 \underline{K}'_{F\Omega_x},$$

with $J_x$ = inertia moment of airplane about the path axis, and $\underline{K}'_{F\Omega_x}$ = coefficient of moment - essentially set up by the wing only - about the path axis due to a rotation $\Omega_x$ about the path axis. Since the angles of attack in question are comparatively small, this factor may be made to equal the $\underline{K}_{F\Omega_x}$ coefficient of the corresponding moment about the longitudinal axis.

For reasons of integration of the above differential equation, this $\underline{K}_{F\Omega_x}$ of the moment about the longitudinal axis is assimilated to a parabola with respect to $\frac{b\Omega_x}{2\ v}$. Now compare the dotted line in Figure 3. We have

$$\underline{K}'_{F\Omega_x} = -\frac{4r}{p^2}\ \frac{b\Omega_x}{2\ v}\left(\frac{b\Omega_x}{2\ v} - p\right),$$

with $p$ and $r$ as denoted in Figure 3. We singled out the moment curve for that angle of attack at which the slope of $m_3$ is greatest, because the magnitude of $m_3$ is, as we have seen, the primary factor in sideslipping.

Now we insert $\frac{b\Omega_x}{2\ v} = U$ and the differential equation reads:

$$\dot{U} = \frac{\gamma\ v\ b\ F\ t_1\ r}{g\ J_x\ p^2}\ U\ (U - p).$$

With a disturbance $\Delta U$ of $U$ magnitude in time interval $t = 0$ as basis, we have:

$$U = \frac{p\ E\ e^{\lambda t}}{E\ e^{\lambda t} - 1} \tag{24}$$

whereby

$$E = \frac{\Delta U}{\Delta U - p}$$

$$\lambda = -\frac{\gamma\ v\ b\ F\ t_1\ r}{g\ J_x\ p}.$$

Now, since $\Omega_x = \dot{\mu}$, equation (24) yields:

$$\mu = \frac{2\ v}{b}\ \frac{p}{\lambda}\ \ln \frac{1 - E\ e^{\lambda t}}{1 - E} \tag{25}$$

With $r = -0.21$, $p + 0.330$ and $\Delta U = 0.031$, our previous example shows

$$\mu = 0.168\ \ln \frac{1 + 0.104\ e^{6.36t}}{1.104}.$$

This solution checks very closely with the numerical integration appended in Figure 18, and again shows that the inception of sideslip is quite satisfactorily reproduced by the autorotation test in the wind tunnel.

In accordance with this example, $\Delta U$ is ordinarily set at +0.031, that is, $\mu_0 = + 0.1$. The $\mu$ values, computed according to the demonstrated method, are compared in Figure 18 with three practical types of airplanes. (References 9 and 10.) One could expect that diversified behavior of these types would become noticeable here with respect to autorotation. But it becomes apparent the angle of bank $\mu$ practically changes in the same way for all these types. This becomes comprehensible upon reflection that $m_3$, and moreover, the inertia moment, are the dominant factors when no autorotation prevails.

Translation by J. Vanier,
National Advisory Committee
for Aeronautics.

## References

1. Fuchs, Richard, and Schmidt, Wilhelm: The Steady Spin. N.A.C.A. Technical Memorandum No. 630, 1931. Translation from Luftfahrtforschung, Feb. 27, 1929, Vol. III, No. 1, pp. 1-18.

2. Fuchs, Richard, and Schmidt, Wilhelm: The Dangerous Flat Spin and the Factors Affecting It. N.A.C.A. Technical Memorandum No. 629, 1931. Translation from Zeitschrift für Flugtechnik und Motorluftschiffahrt, July 14 & 28, 1930, Vol. 21, Nos. 13 & 14.

3. Reissner: Wissenschaftliche Fragen der Flugtechnik, Deutsche Math. Vereinigung 1909, p. 31.

4. Batson, A. S., Williams, S. H., and Halliday, A. S.: Experiments on a Model of a Fokker (F.VII) Monoplane Wing. British A.R.C. R&M No. 1059, Sept., 1926. Pt.II.

5. Fuchs, Richard, and Schmidt, Wilhelm: Aerodynamic Forces and Moments at Large Angles of Attack and Their Dependence on the Shape of the Wing. Zeitschrift für Flugtechnik und Motorluftschiffahrt, Jan. 14, 1930, Vol. 21, No. 1.

References (continued)

6. Schmidt, Wilhelm: Development of an Airplane Which is Proof against Autorotation and Capable of Steep Landing. Submitted Dec. 16, 1929, to the Technische Hochschule, Berlin, as a doctor's dissertation; accepted Dec. 17, 1930. (To be published later.)

7. Aeronautical Research Committee (British): The Lateral Control of Stalled Aeroplanes. General report by the Stability and Control Panel. British A.R.C. R&M No. 1000, Sept., 1925.

8. Jones, B. Melvill, and Trevelyan, A.: Step by Step Calculations upon the Asymmetric Movements of Stalled Aeroplanes. British A.R.C. R&M No. 999, Oct., 1925.

9. Irving, H. B., Batson, A. S., Townend, H. C. H., and Kirkup, T. A.: Some Experiments on a Model of a B.A.T. Bantam Aeroplane with Special Reference to Spinning Accidents.
Part I-Longitudinal Control and Rolling Experiments.
" II-Experiments on Forces and Moments (including rudder control).
British A.R.C. R&M No. 976, Nov., 1925.

10. Bradfield, F. B.: Lateral Control of Bristol Fighter at Low Speeds. Measurement of Rolling and Yawing Moments of Model Wings Due to Rolling. British A.R.C. R&M No. 787, Jan., 1921.

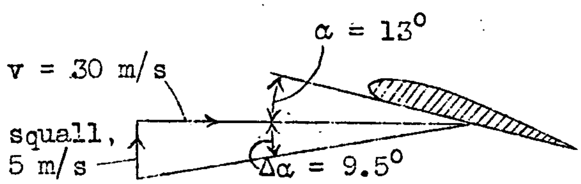


Fig.1 Increase in angle of attack due to a vertical squall.

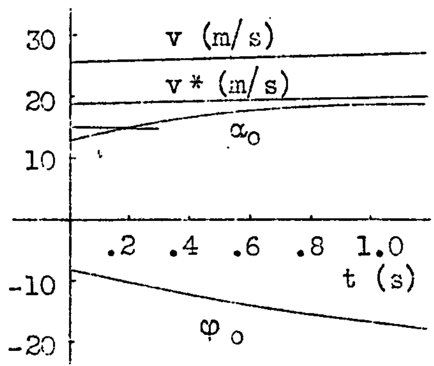


Fig. 2 Increase in angle of attack due to a horizontal squall.
v = speed of flight, v* = reduced relative wind velocity.

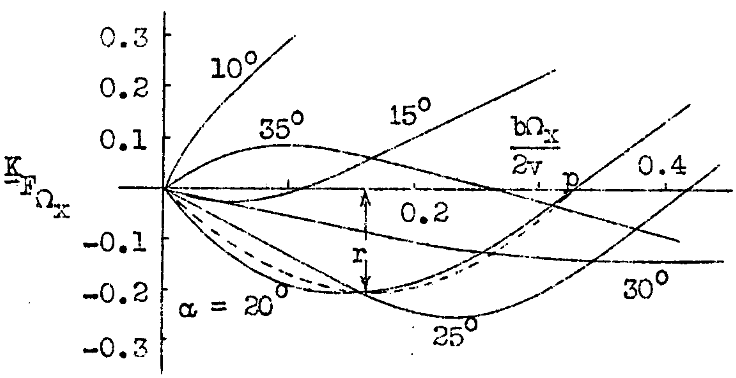


Fig.3 Coefficient of wing moment about the longitudinal axis plotted against $\frac{b\Omega_x}{2v}$, and $\alpha$ as parameter.

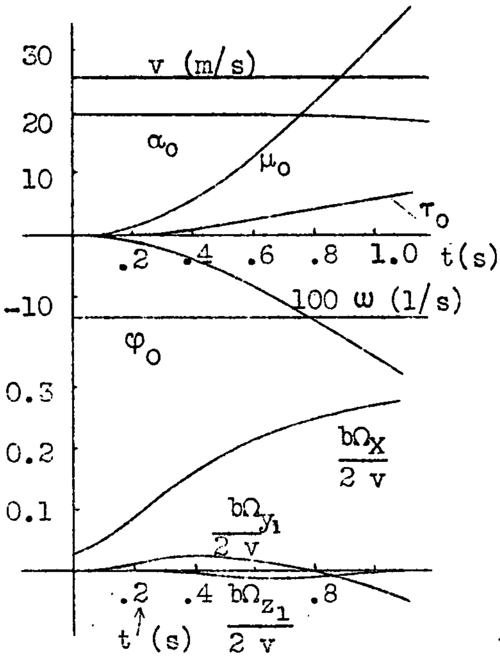


Fig. 4 Temporary course of the variable following a passing asymmetric disturbance. $\dot{\mu}_o = +0.1$ (1/s)

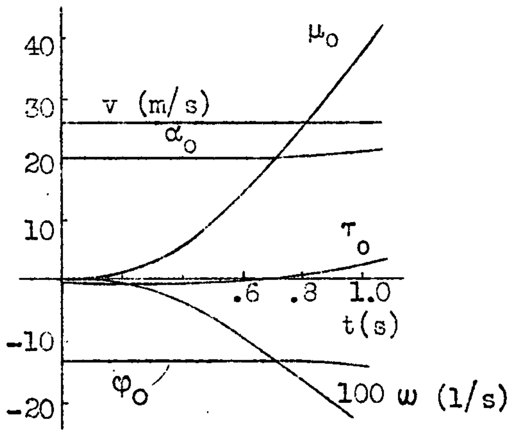


Fig. 5 Temporary course of the variable following a passing asymmetric disturbance. $\dot{\tau}_o = -0.1$ (1/s)

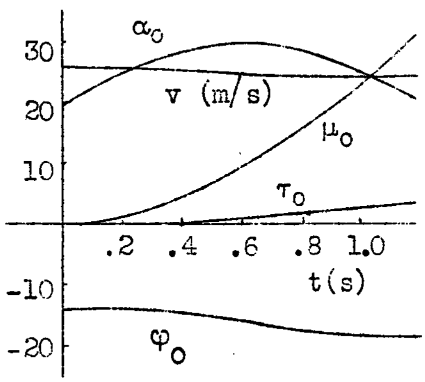


Fig. 6 Temporary course of the variable following a passing combined disturbance $\dot{\mu}_o = +0.1$ (1/s) and $\dot{\alpha}_o = +0.5$ (1/s)

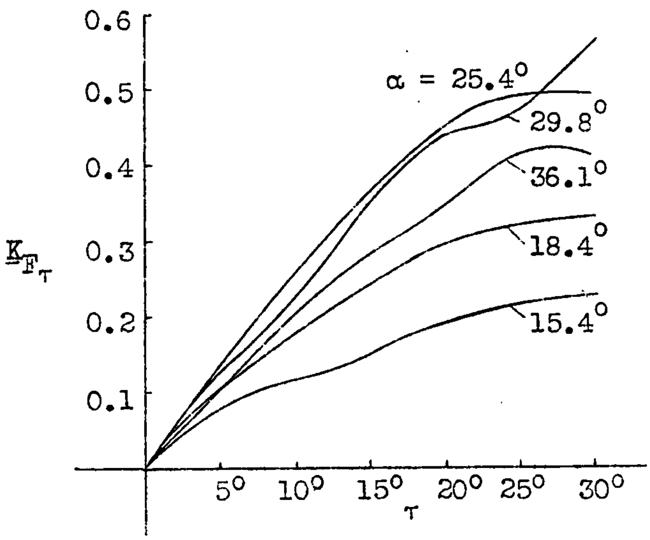


Fig. 7

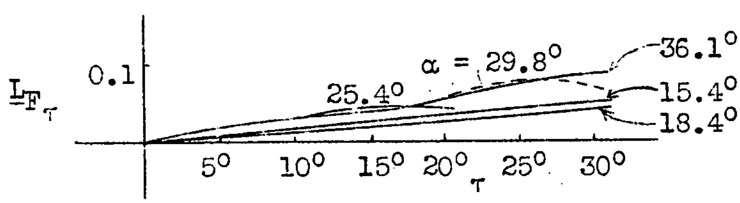


Fig. 8

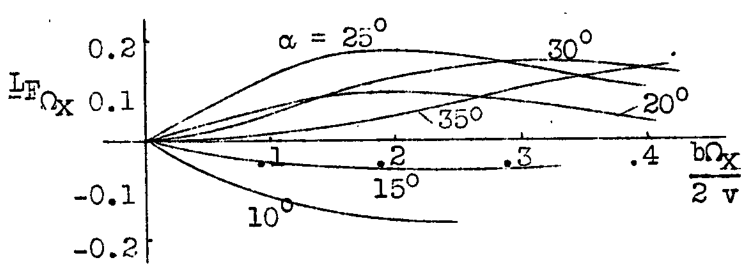


Fig. 9 Coefficient of wing moment about the normal axis against $\frac{b\Omega_x}{2\,v}$ with, α shown as parameter

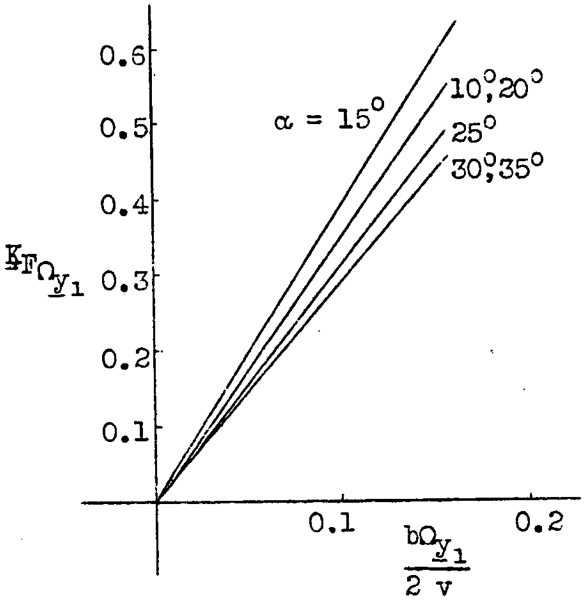


Fig.10 Coefficient of wing moment about the longitudinal axis against $\frac{b\Omega_{y_1}}{2\,v}$ with $\alpha$ shown as parameter.

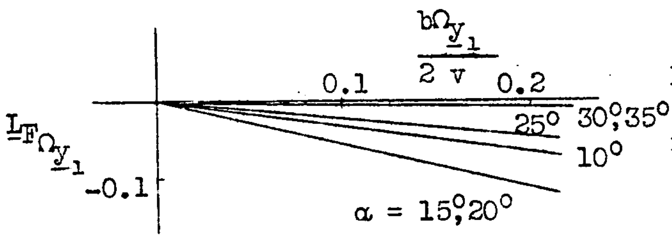


Fig. 11 Coefficient of wing moment about the normal axis against $\frac{b\Omega_{y_1}}{2\,v}$, and $\alpha$ as parameter.

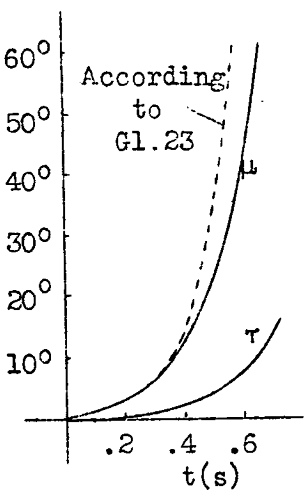


Fig. 12 Increase in angles of bank and yaw following a passing asymmetric disturbance.
$\dot{\mu}_0 = +0.1$ (1/s)

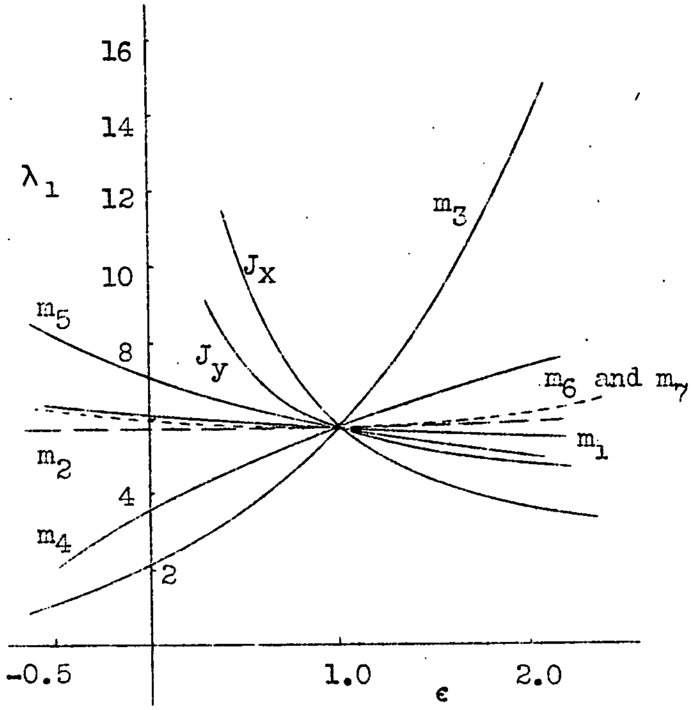


Fig. 13, The positive root $\lambda_1$ plotted against $\epsilon$.

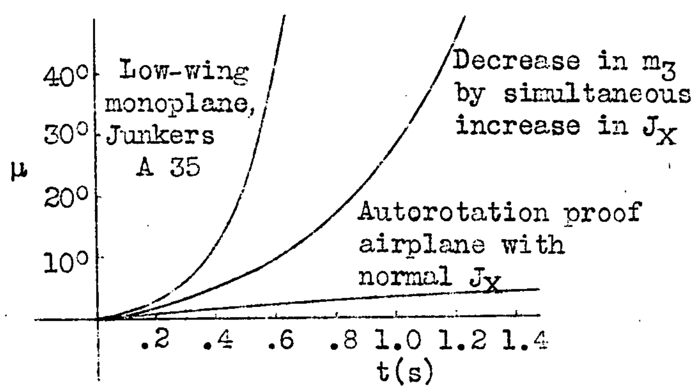


Fig. 14, Increase in angle of bank following a passing asymmetric disturbance $\dot{\mu}_0 = +0.1$ (1/s)

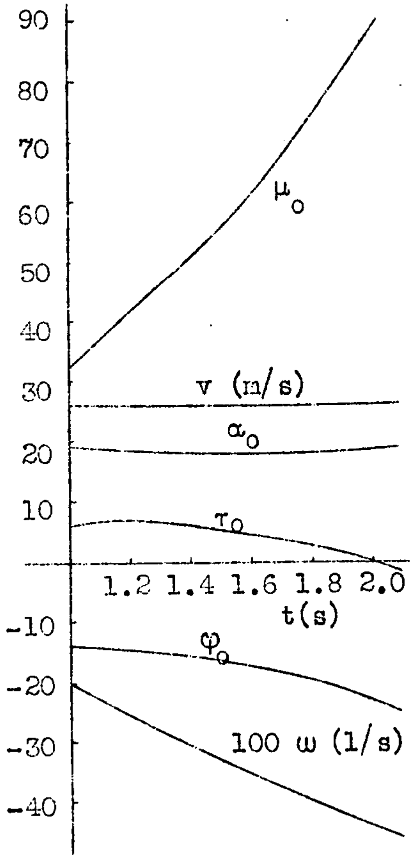


Fig. 15 Temporary course of the variable following an aileron displacement (continuation of Fig.4)

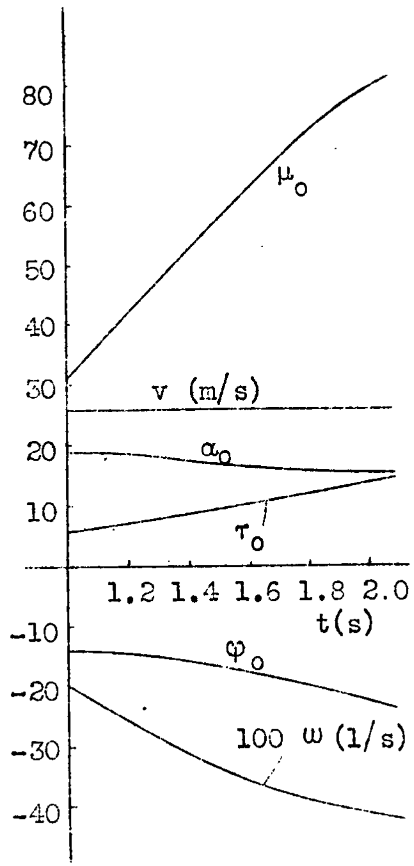


Fig. 16. Temporary course of the variable following a rudder displacement. (continuation of Fig.4)

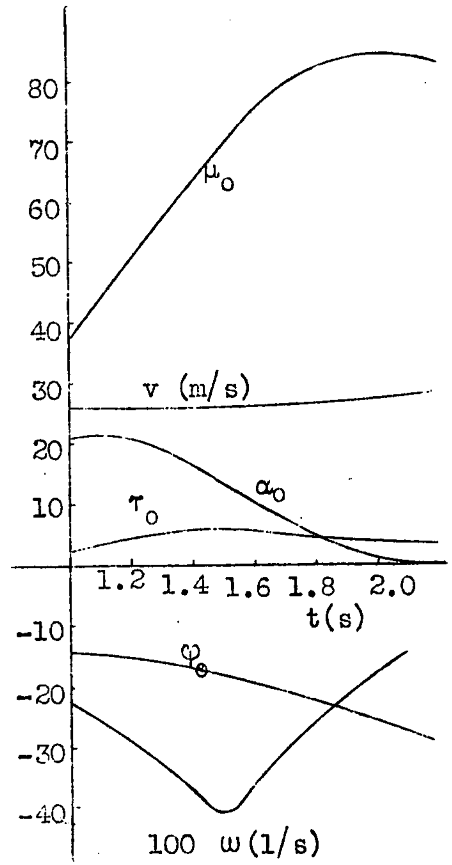


Fig. 17, Temporary course of the variable following an elevator displacement (downward).(continuation Fig.5)

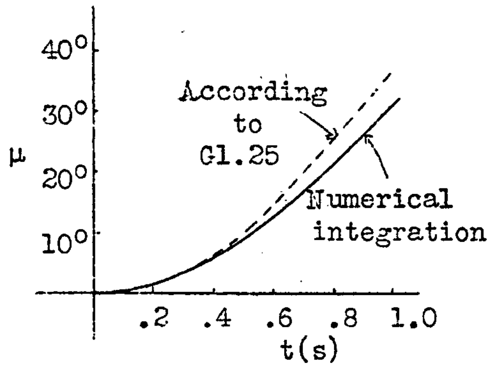


Fig. 18, Increase in angle of bank following a passing asymmetric disturbance $\dot{\mu}_0 = +0.1$ (1/s).

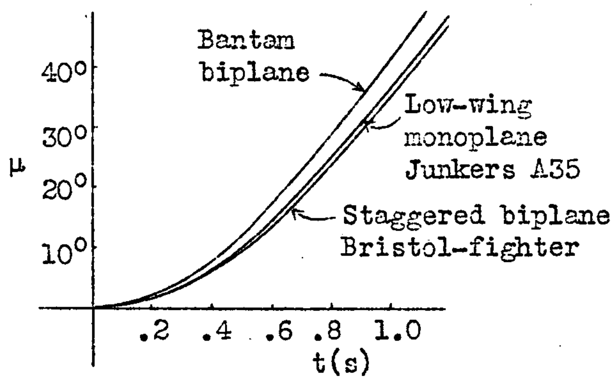


Fig. 19, Increase in angle of bank following a passing asymmetric disturbance $\dot{\mu}_0 = +0.1$ (1/s).